PHYSICAL REVIEW D **86,** 046007 (2012)

# Holographic superconductors with $z = 2$ Lifshitz scaling

Yanyan Bu*

*State Key Laboratory of Theoretical Physics, Institute of Theoretical Physics, Chinese Academy of Science, Beijing 100190, People's Republic of China and Max-Planck-Institut fr Physik (Werner-Heisenberg-Institut), Fhringer Ring 6, 80805 Munchen, Germany*

(Received 22 June 2012; published 20 August 2012)

We use gauge/gravity duality to explore strongly coupled superconductors with dynamical exponent $z = 2$. In the probe limit we numerically establish background solutions for the matter fields and plot the condensate versus the dimensionless temperature. We then investigate electromagnetic perturbations in order to compute the ac conductivity and also calculate the spectral function. Our results for the condensate and conductivity are qualitatively similar to those of the anti-de Sitter (AdS) superconductor. However, we find that (for both the $s$-wave and $p$-wave) the condensate does not approach a constant at very low temperature and the conductivity goes to 1 from below but never exceeds it in the high frequency limit, in contrast to the AdS black hole. We do not see a peak at nonzero frequency in the imaginary part of the ac conductivity along the $x$ direction for the $p$-wave case. These features are due to the nontrivial dynamical exponent. To be specific, the black hole geometry considered in this work is anisotropic between space and time, very different from the Schwarzschild-AdS black hole, which results in different asymptotic behaviors of temporal and spatial components of gauge fields than those in the Schwarzschild-AdS black hole.

DOI: 10.1103/PhysRevD.86.046007 PACS numbers: 11.25.Tq

## I. INTRODUCTION

The application of gauge/gravity duality [1] to the investigations of strongly coupled systems has gained broad interest ranging from QCD phenomena at low energy to strongly correlated condensed matter physics; see, e.g., Ref. [2] for some recent reviews. Holographic superconductors have been constructed in Refs. [3,4] by putting the Abelian-Higgs model or SU(2) gauge field into the anti-de Sitter (AdS) black hole spacetime. When the Hawking temperature is decreased to a critical value, the black hole becomes unstable against small perturbations and develops hair by condensing some field to stabilize the system. This can be considered as the holographic realization of the superconducting phase transition. This kind of construction for holographic superconductors takes the (asymptotically) AdS black hole spacetime as the starting point. According to the AdS/CFT correspondence, the AdS black hole geometry corresponds to a relativistic conformal field theory (CFT) at finite temperature. However, many condensed matter systems do not have relativistic symmetry and it is therefore very natural and interesting to generalize these holographic superconducting models to nonrelativistic situations.

On the other hand, inspired by the dynamical exponent in condensed matter physics near the critical point, many papers have appeared on the construction of black hole geometries with anisotropic scaling, such as the Lifshitz black hole. The dual geometry of Lifshitz fixed points was first proposed in Ref. [5] and then generalized to finite temperature in Ref. [6]. In short, we now have a geometrical realization of a strongly coupled anisotropic field theory at finite temperature. It is expected that nonrelativistic AdS/CFT will help us to understand some puzzles in unconventional condensed matter physics.[1]

In Ref. [8] a variety of strange metallic behaviors have been realized by using gravity duals of the Lifshitz fixed points and some string theoretical realizations of this geometry have been proposed in that paper.[2] More recently, holographic fermions have been studied in Ref. [10] to produce a non-Fermi liquid behavior. With these studies in mind, we now generalize holographic superconductors under the relativistic AdS/CFT framework to the Lifshitz black hole geometry in order to explore the effects of the dynamical exponent and also in the hope to distinguish some universal properties of holographic superconductors. In fact, holographic $s$-wave superconductors with a Lifshitz fixed point have been constructed in Refs. [11,12] and in Hořava-Lifshitz gravity in Ref. [13]. However, the work of Brynjolfsson *et al.* [12] produced only the condensate and the results of Sin *et al.* [11] seemed surprising, especially the very small real part of the ac conductivity. We therefore more carefully study these systems here in order to clarify some confusions which appeared in Ref. [11] and also reveal some properties of $p$-wave superconductors with Lifshitz scaling.

Although there is a dynamical exponent, which makes the Lifshitz geometry behave quite differently from

*yybu@mpp.mpg.de

[1]Actually, there are many works that use these kinds of nonrelativistic metrics to reveal some strange features of a condensed matter system; see Ref. [7] for an incomplete list.

[2]Another string theory realization of Lifshitz-like fixed points was investigated in Ref. [9].

 

asymptotically AdS spacetime, we find that qualitative behaviors of holographic superconductors with Lifshitz scaling (for both $s$-wave and $p$-wave) are basically the same as those of the AdS black hole case. The condensate has mean-field behavior near the critical temperature. A gap does appear when decreasing the temperature, which manifests once looking at the real part of the ac conductivity. There is also a delta peak near zero frequency for the conductivity, which is a signal of DC superconductivity. The real part of the conductivity approaches one in the high frequency limit where the imaginary part goes to zero. These common characteristics of holographic superconductors appear to be robust phenomena and can be taken as universal properties of gauge/gravity duality when applied to the study of strongly coupled condensed matter systems.

We also find some other interesting features in our work. The first is that all the condensates do not approach some constant in the zero temperature limit compared to the Bardeen-Cooper-Schrieffer (BCS) superconductor and the AdS black hole holographic superconductors. The real part of the conductivity never exceeds one and the imaginary part of the conductivity just approaches zero from above but never goes below zero in the high frequency limit. What is more striking is that there is no pole at nonzero frequency for the imaginary part of the ac conductivity $\sigma_{xx}(\omega)$ in the $p$-wave case. We therefore attribute these nontrivial features to the effect of the Lifshitz scaling. More specifically, the black hole geometry considered in this work is anisotropic between space and time, very different from the AdS black hole, which results in different asymptotic behaviors of temporal and spatial components of gauge fields than previous conclusions in an AdS black hole.

Our paper is organized as follows. In Sec. II we briefly review basic aspects of asymptotic Lifshitz black holes for further studies. Section III is concerned with the construction of $s$-wave superconductors in the Lifshitz black hole geometry. With the numerical solutions one can plot the condensate as well as the free energy difference between the normal and superconducting phases versus the dimensionless temperature. We find that the free energy difference is always greater than zero when below the critical temperature $T_c$, which proves that the superconducting phase is at least thermodynamically stable. Then we move on to investigate the electromagnetic fluctuations of the system and numerically calculate the ac conductivity using linear response theory. The spectral functions for the electromagnetic perturbations are calculated as well. In Sec. IV the corresponding results for the $p$-wave superconductor are presented. A short summary is given in Sec. V.

## II. HOLOGRAPHIC SETUP: THE GRAVITY DUAL OF THE LIFSHITZ FIXED POINT

In this section, we concisely provide some backgrounds for the gravity dual of the Lifshitz fixed point. As mentioned in Sec. I, there exist field theories with anisotropic scaling symmetry between the temporal and spatial coordinates. This is found for example in some condensed matter systems near the critical point,

$$t \to \lambda^z t, \qquad x^i \to \lambda x^i, \tag{1}$$

where $z$ is called the dynamical exponent. One geometrical realization of this scaling symmetry comes from the generalized gauge/gravity duality: we can map this scaling symmetry in the field theoretical side to some geometrical symmetry in the gravity side. Then it is straightforward to write down the metric with this type of scaling symmetry,

$$ds^2 = L^2\left(-r^{2z}dt^2 + r^2\sum_{i=1}^{d} dx_i^2 + \frac{dr^2}{r^2}\right), \tag{2}$$

where $0 < r < \infty$ and $L$ is the radius of curvature of the geometry. This geometry was first proposed in Ref. [5] where the action sourcing this geometry was also given. The scale transformation takes the following form:

$$t \to \lambda^z t, \qquad x^i \to \lambda x^i, \qquad r \to \frac{r}{\lambda}. \tag{3}$$

When $z = 1$, the above geometry reduces to the usual $\mathrm{AdS}_{d+2}$ spacetime and the symmetry group is enlarged to $SO(d+1,2)$.

According to the gauge/gravity duality, to put the dual field theory at finite temperature one can study the metric with a black hole and the Hawking temperature of the black hole is identified as the temperature of the dual field theory. It is therefore of great interest to construct a finite temperature version of the above geometry, i.e., the so-called Lifshitz black hole. However, it is difficult to obtain analytic black hole solutions in Lifshitz spacetimes. There are some attempts to construct Lifshitz black holes[3] and we here follow the work of Bertoldi *et al.* [6]. It was found that action of the form

$$S = \frac{1}{16\pi G_{d+2}}\int d^{d+2}x\sqrt{-g} \times\left(R - 2\Lambda - \frac{1}{2}\partial_\mu\phi\partial^\mu\phi - \frac{1}{4}e^{\lambda\phi}\mathcal{F}_{\mu\nu}\mathcal{F}^{\mu\nu}\right), \tag{4}$$

where $\Lambda$ is the cosmological constant, $\phi$ is a massless scalar and $\mathcal{F}_{\mu\nu}$ is an Abelian gauge field strength. This admits the following black hole geometry:

$$ds^2 = L^2\left(-r^{2z}f(r)dt^2 + r^2\sum_{i=1}^{d} dx_i^2 + \frac{dr^2}{r^2 f(r)}\right), \tag{5}$$

$$f(r) = 1 - \frac{r_0^{z+d}}{r^{z+d}}, \qquad \Lambda = -\frac{(z+d-1)(z+d)}{2L^2}. \tag{6}$$

To support the above black hole geometry, one also needs to give the backgrounds for $\phi$ and $\mathcal{F}_{rt}$,

[3]See Refs. [14,15] for an incomplete list of the constructions of black hole geometries with anisotropic scaling symmetry.

$$e^{\lambda\phi} = r^{-2d}, \qquad \lambda^2 = \frac{2d}{z-1}, \qquad \mathcal{F}_{rt} = q_0 r^{z+d-1},$$
$$q_0^2 = 2L^2(z-1)(z+d). \tag{7}$$

Evidently, choosing the dynamical exponent $z$ to be 1 reduces the Lifshitz black hole to the Schwarzschild-AdS black hole in $d+2$ dimensions. The Hawking temperature and the entropy of the black hole are

$$T = \frac{z+d}{4\pi} r_0^z, \qquad S_{en} = \frac{L^d V_d}{4G_{d+2}} r_0^d, \tag{8}$$

where $V_d$ denotes the volume of the $d$-dimensional space.

We do a coordinate transformation $u = r_0/r$ to map the holographic direction $r$ into a finite interval [0, 1] as we find that it is more convenient to use this coordinate system when carrying out numerical calculations. We will focus on a four-dimensional bulk theory and choose the dynamical exponent $z = 2$. With these choices, the bulk geometry is reduced to

$$ds^2 = L^2\left(-\frac{r_0^{2z}}{u^{2z}} f(u) dt^2 + \frac{r_0^2}{u^2}(dx^2 + dy^2) + \frac{du^2}{u^2 f(u)}\right),$$
$$f(u) = 1 - u^{z+2}. \tag{9}$$

In this new coordinate system, the horizon is located at $u = 1$ and $u = 0$ denotes the conformal boundary where the dual field theory lives.

## III. HOLOGRAPHIC *S*-WAVE SUPERCONDUCTORS WITH LIFSHITZ SCALING

This section and the next are the central parts of our work. In this section we focus on aspects of $s$-wave superconductor. In Sec. III A we list the equations of motion for the background fields and solve them by a shooting method. Section III B is devoted to the studies of the electromagnetic perturbations of the system.

### A. Solution for the background fields

In Ref. [16], it was shown that a charged AdS black hole supports charged scalar hair if the charge is large enough. Later this idea was generalized to the neutral AdS black hole in Ref. [3], which is the first model of an $s$-wave holographic superconductor. More specifically, it is constructed from the Abelian-Higgs model in the AdS black hole background. The action for this system is

$$S = \int d^4x\sqrt{-g}\left(R + \frac{6}{L^2} - \frac{1}{4}F_{\mu\nu}F^{\mu\nu} - |\partial_\mu\Psi - iqA_\mu\Psi|^2 - V(|\Psi|)\right), \tag{10}$$

where we choose $V(|\Psi|) = m^2|\Psi|^2$ for simplicity. This is the minimal Lagrangian of the gravitational dual which holographically describes a superconducting phase transition. As mentioned before, we work in the probe limit, i.e., the black hole geometry is fixed and feels no effect of the matter fields. Above the critical temperature, the black hole background is stable and the scalar field $\Psi$ can be set to zero. This corresponds to the normal phase. When the temperature is decreased to the critical value, the black hole background becomes unstable against small perturbations and the scalar field wants to condense in order to stabilize the system. Once this happens, the black hole develops hair and the system goes through a superconducting phase transition. The scalar field $\Psi$ holographically models the order parameter of a conventional superconductor and gets a nontrivial profile only in the superconducting phase. As the AdS/CFT correspondence maps a strongly coupled field theory to a weakly coupled gravity system, the holographic method is expected to give a description of strongly coupled superconductors in contrast to the conventional BCS theory. However, it is still far from being clear as to the pairing mechanism in holographic superconductors. Due to the conformal characteristic of the AdS space, the chemical potential is usually introduced to explicitly break the conformal invariance and to make the temperature scale meaningful. This is achieved by turning on the time component of the U(1) gauge field.

Having fixed the black hole geometry, the equations of motion for $A_\mu$ and $\Psi$ can be easily extracted from the Euler-Lagrange equations and are listed here for further studies in later subsections,

$$\frac{1}{\sqrt{-g}}\partial_\mu(\sqrt{-g}F^{\mu\nu}) = iq[\Psi^*(\partial^\nu\Psi - iqA^\nu\Psi) - \Psi(\partial^\nu\Psi^* + iqA^\nu\Psi^*)], \tag{11}$$

$$\partial_\mu[\sqrt{-g}(\partial^\mu\Psi - iqA^\mu\Psi)] = \sqrt{-g}[V'(|\Psi|)\frac{\Psi}{2|\Psi|} + iqA^\mu(\partial_\mu\Psi - iqA_\mu\Psi)]. \tag{12}$$

From the radial component of Eq. (11) one can show that the scalar field can be taken as real. Therefore, the ansatz for the backgrounds of the gauge and scalar fields are

$$A = \phi(u)dt, \qquad \Psi = \psi(u). \tag{13}$$

Recalling the Lifshitz black hole background given in Eq. (9), we obtain the following equations of motion:

$$\phi'' + \frac{z-1}{u}\phi' - \frac{2\psi^2}{u^2 f(u)}\phi = 0, \tag{14}$$

$$\psi'' + \left[\frac{f'(u)}{f(u)} - \frac{z+1}{u}\right]\psi' + \frac{u^{2z-2}\phi^2}{f^2(u)}\psi - \frac{m^2L^2}{u^2 f(u)}\psi = 0, \tag{15}$$

where we have for simplicity chosen the scalar potential $V(\Psi)$ as $m^2\Psi^2$, giving mass to $\Psi$, and set the charge $q^2L^2 = 1$. The prime in these equations denotes a derivative

with respect to $u$ and this notation will be used in the following.

Before continuing, some remarks are in order. Actually, in Eqs. (14) and (15), we have rescaled the fields $\phi$ and $\psi$ for convenience. When the dynamical exponent $z$ is nontrivial, the rescaling is different between $\psi$ and $\phi$,

$$\phi \to \frac{z+2}{4\pi T}\phi, \qquad \psi \to \left(\frac{z+2}{4\pi T}\right)^{1/z}\psi. \tag{16}$$

The superconducting phase transition is a spontaneous breaking of the electromagnetic symmetry, which should be reflected in the holographic description in some sense. Strictly speaking, the gauge symmetry in the bulk corresponds to a global symmetry on the boundary field theory according to gauge/gravity duality and therefore we have no electromagnetic symmetry on the boundary. Then the holographic superconductor model should at most be thought of as holographic superfluidity. However, as discussed in Ref. [3] this model can produce many features of superconductors and we can ignore this subtlety.

We now have a look at the asymptotic behaviors of the background fields $\phi$ and $\psi$. Near the horizon, one must have $\phi(1) = 0$ for its norm to be finite and the scalar field should also be finite there. Near the conformal boundary, we have the following asymptotic behavior from the Frobenius analysis of Eqs. (14) and (15) near the singularity $u = 0$:

$$\begin{aligned} &\phi(u \to 0) \sim \mu + \rho u^{2-z} \qquad (z \neq 2) \quad \text{or} \\ &\phi(u \to 0) \sim \rho + \mu \log u \qquad (z = 2), \end{aligned} \tag{17}$$

and

$$\psi(u \to 0) \sim \psi^{(\nu_+)}u^{\nu_+} + \psi^{(\nu_-)}u^{\nu_-}, \tag{18}$$

where the scaling dimension $\nu_\pm$ of the scalar operator $\mathcal{O}$ dual to the bulk scalar $\psi$ is given by $\nu_\pm = \frac{z+2\pm\sqrt{(z+2)^2+4m^2}}{2}$. It is explicit that the Breitenlohner-Freedman bound for the scalar mass in the Lifshitz background is now changed to $m^2 \geq -\frac{(z+2)^2}{4}$ for four-dimensional bulk. To obtain explicit behavior for these two fields near the conformal boundary, we need to specify the mass squared of the scalar field and the dynamical exponent. We here choose $z = 2$ and $m^2 = 0, -3$ (which are both above the Breitenlohner-Freedman bound).

For the exponent $z = 2$, the boundary behavior of the $\phi(u)$ field has a logarithmic term due to degenerate indices of Eq. (14) near the conformal boundary $u = 0$. Now the physical result is also changed; we should identify the constant term $\rho$ as the charge density, as it is a normalizable mode with respect to the logarithmic term, and the non-normalizable logarithmic term $\sim\mu \log[u]$ as the chemical potential. Fortunately, this happens only for the time component of the gauge field and the final result for the conductivity does not change too much. We will come to see this when studying the ac conductivity along the $x$ direction for the $p$-wave case.

From the boundary behavior of the scalar field $\psi$, we can directly read off the expectation value of the dual operator $\mathcal{O}$. When $m^2 = 0$, the indices $\nu = 0$ and 4,

$$\psi(u \to 0) \sim \psi^{(0)} + \psi^{(4)}u^4. \tag{19}$$

To make the superconducting phase transition a spontaneous breaking of symmetry, we should impose that

$$\psi^{(0)} = 0 \quad \text{and} \quad \langle \mathcal{O}_4 \rangle \sim \psi^{(4)}. \tag{20}$$

Therefore, there is only one theory for this choice of the scalar mass squared.

While for $m^2 = -3$ the indices $\nu = 1$ or 3,

$$\psi(u \to 0) \sim \psi^{(1)}u + \psi^{(3)}u^3. \tag{21}$$

Evidently, the two modes in the above equation are both normalizable according to Klebanov and Witten [17], and in order to make the theory stable, we should either impose

$$\psi^{(1)} = 0 \quad \text{and} \quad \langle \mathcal{O}_3 \rangle \sim \psi^{(3)} \tag{22}$$

or

$$\psi^{(3)} = 0 \quad \text{and} \quad \langle \mathcal{O}_1 \rangle \sim \psi^{(1)}. \tag{23}$$

We now have two theories for $m^2 = -3$ corresponding to dimension 1 or dimension 3 order parameters, respectively. In the following analysis, we will concentrate on the dimension 3 case because we find that the ground state of the dimension 1 theory is numerically unstable.

With the boundary conditions mentioned above, we can now use a numerical shooting method to solve the coupled nonlinear Eqs. (14) and (15). The condensates corresponding to operators $\mathcal{O}_3$ and $\mathcal{O}_4$ are plotted in Fig. 1.

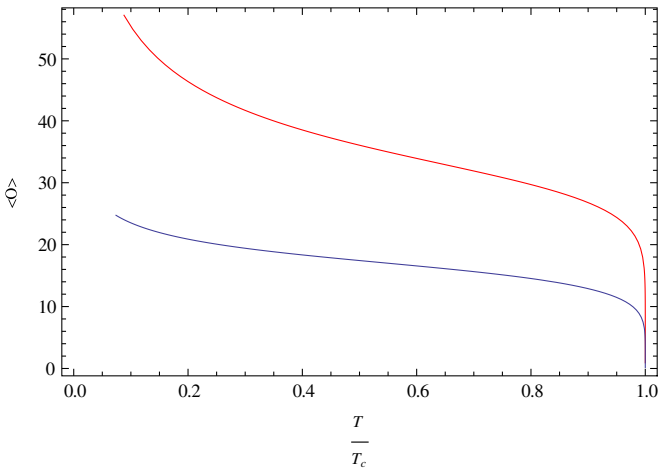


FIG. 1 (color online). The condensates of the $s$-wave superconductor for the dimensionless three-dimensional operator $\mathcal{O}_3$ (blue): $\sqrt[3]{\langle\mathcal{O}_3\rangle/T_c}$ and four-dimensional operator $\mathcal{O}_4$ (red): $\sqrt[4]{\langle\mathcal{O}_4\rangle/T_c}$.

From this figure, we see that the condensates go to zero at the critical temperature $T_c$. However, they do not approach some fixed constants as the temperature $T \to 0$, which is different from both the conventional BCS theory of weakly coupled superconductors and AdS black hole holographic superconductors. We may attribute this effect to the nontrivial dynamical exponent $z \neq 1$. We also find that the expectation values for the operators $\sqrt[3]{\langle \mathcal{O}_3 \rangle}$ and $\sqrt[4]{\langle \mathcal{O}_4 \rangle}$ are much larger than the BCS predictions at zero temperature. This is consistent with the results of AdS black hole holographic superconductors. Perhaps this is due to the fact that the strongly interacting nature of the holographic superconductor contrasts the BCS theory.

In the mean field theory for the superconductor, the order parameters have a square root behavior near the critical temperature $T_c$,

$$\langle \mathcal{O} \rangle \sim (T_c - T)^{1/2}. \tag{24}$$

By fitting these curves, we find the mean-field behavior also holds in our results. Specifically, for the dimension 3 theory:

$$\langle \mathcal{O}_3 \rangle \approx (18.9117 T_c)^3 (1 - T/T_c)^{1/2} \quad \text{when } T \to T_c, \tag{25}$$

where the critical temperature $T_c \approx 0.0351935\mu$. For the dimension 4 theory:

$$\langle \mathcal{O}_4 \rangle \approx (35.5940 T_c)^4 (1 - T/T_c)^{1/2} \quad \text{as } T \to T_c, \tag{26}$$

with the critical temperature $T_c \approx 0.0229931\mu$.

The relation between the chemical potential and charge density is plotted in Fig. 2. We see that the profile has a small deviation from the linear behavior in the superconducting phase. There is one critical value for the chemical potential where the charge density becomes nonzero. This is actually the critical point where the superconducting phase transition occurs.

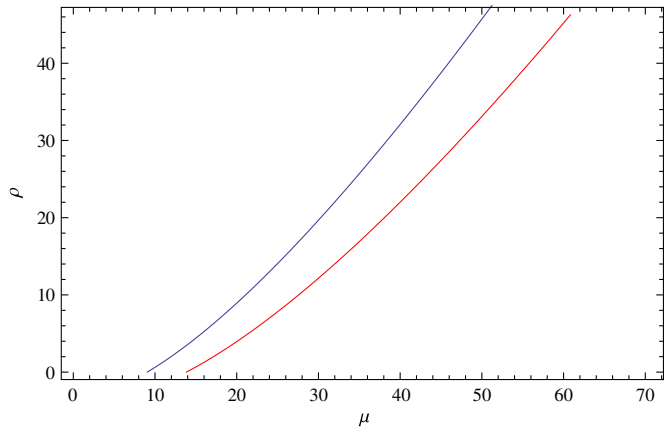


FIG. 2 (color online). The profile of the charge density as a function of the chemical potential in the superconducting phase for the $s$-wave superconductors. The blue line represents the dimension 3 theory and the red line represents for the dimension 4 theory.

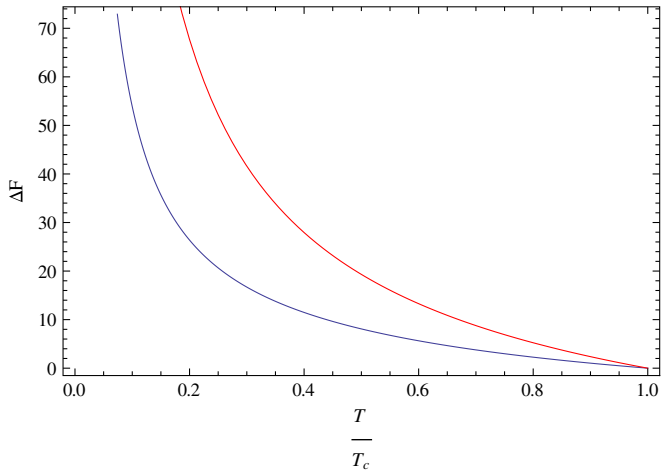


FIG. 3 (color online). The dimensionless free energy difference between the normal and the superconducting phases of the $s$-wave superconductor for $\mathcal{O}_3$ (blue line) and $\mathcal{O}_4$ (red line) theories, respectively.

At the end of this subsection, we plot the free energy for the two theories, which can be taken as one piece of evidence that the superconducting phase transition does happen when the temperature is decreased to the critical one. With the equations of motion for the backgrounds $\phi$ and $\psi$, we can reduce the action (10) to some simpler expression by integrating by parts. Then, the free energy difference between the normal and superconducting phases is

$$\begin{aligned} \Delta \Xi_{N-SC} &= \frac{V_2}{2g_4^2} r_0^{z+2} \int_0^1 du \frac{u^{z-1}}{f(u)} (\phi(u)\psi(u))^2 \\ &\equiv \frac{V_2}{2g_4^2} r_0^{z+2} \Delta F. \end{aligned} \tag{27}$$

Figure 3 is for the plot of the free energy difference. Clearly, the superconducting phase is thermally stable when $T < T_c$.

### B. Fluctuation analysis: ac conductivity and the spectral function

To calculate the ac conductivity of this system, we need to study the electromagnetic perturbation of the above background (here, we do not consider fluctuation of the scalar field). For the $s$-wave superconductor, the conductivity is isotropic and it is therefore equivalent to study any spatial component of the gauge field. We here choose radial gauge for the electromagnetic fluctuation, i.e., $a_u = 0$. For the purpose of the ac conductivity, we take the following ansatz for the electromagnetic perturbation $a_x(t, \vec{x}, u)$:

$$a_x(t, \vec{x}, u) = e^{-i\omega t} a_x(u), \tag{28}$$

where we have taken spatial momentum to zero. Then, the equation of motion for $a_x(u)$ is

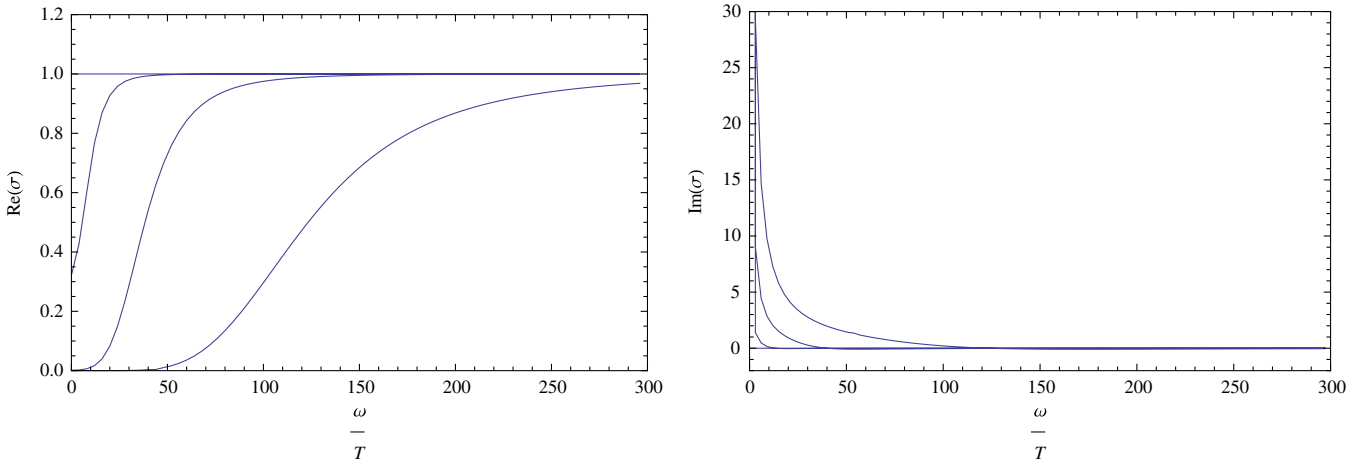


FIG. 4 (color online). The real (imaginary) part of the ac conductivity of the $s$-wave superconductor for the dimension 3 theory at $T/T_c = 1.0, 0.798694, 0.269798, 0.0864351$ from top to bottom (bottom to top).

$$a_x'' + \left[\frac{f'(u)}{f(u)} - \frac{z-1}{u}\right]a_x' + \left[\frac{\tilde{\omega}^2 u^{2z-2}}{f(u)^2} - \frac{2\psi^2}{u^2 f(u)^2}\right]a_x = 0, \tag{29}$$

where the dimensionless frequency $\tilde{\omega}$ is defined as $\tilde{\omega} = (z+2)\omega/4\pi T$. According to the linear response theory, the conductivity is given by the Kubo formula,

$$\sigma(\omega) = \frac{G(\omega, \vec{k}=0)}{i\omega}, \tag{30}$$

where the retarded Green's function $G(\omega, \vec{k}=0)$ for the operator dual to gauge field can be computed according to the prescription given in Ref. [18].

Near the horizon, we should take the ingoing wave boundary condition for the electromagnetic field fluctuation in order to calculate the retarded Green's function,

$$a_x(u) = (1-u)^{-i\tilde{\omega}/4}[1 + a_x^1(1-u) + a_x^2(1-u)^2 + a_x^3(1-u)^3 + \cdots], \tag{31}$$

where we have set the scale of $a_x$ to be one by making use of the linearity of the fluctuation equation. The coefficients in the above expansion can be uniquely determined once the background $\psi$ and the frequency $\tilde{\omega}$ are specified.

Near the conformal boundary $u = 0$, the general solution to the fluctuation is of the form

$$a_x(u) = A_x^0 + A_x^1 u^2 + \cdots. \tag{32}$$

The conductivity can be expressed as

$$\sigma(\omega) = \frac{1}{i\omega}\frac{A_x^1}{A_x^0} \tag{33}$$

by using the Kubo formula (30). By the way, we also give the definition of the spectral function $\mathcal{R}$ plotted later,

$$\mathcal{R} = -2\,\mathrm{Im}G(\omega, \vec{k}=0) = -2\frac{A_x^1}{A_x^0}. \tag{34}$$

Generically, the equation of motion for the electromagnetic fluctuation (29) cannot be solved analytically due to the presence of the scalar field. The philosophy of the numerical method is that we can use the power series solution as in Eq. (31) and do numerical integration from the horizon to the conformal boundary. Then we can extract the coefficients $A_x^0$ and $A_x^1$ and therefore get the conductivity. Our numerical results for the ac conductivity are plotted in Figs. 4 and 5. From the plots, we find that the real part of the conductivity approaches one in the high frequency limit, which is equal to the results of the normal phase. This is explicit when taking a look at Eq. (29): the effect of the condensed field $\psi$ can be neglected at large $\tilde{\omega}$. Compared to the result for the conductivity in Ref. [2], our result is of order 1 although these profiles are qualitatively similar. We found that the results for dimension 3 and dimension 4 theory are qualitatively the same. We also see that a gap forms as the temperature is lowered and the gap gets increasingly deeper until the conductivity is exponentially small, which is the same as the AdS superconductor [3].

In the imaginary part of the conductivity, there is a pole at zero frequency. This can be explained from the Kramers-Krönig relation

$$\mathrm{Im}[\sigma(\omega)] = -P\int_{-\infty}^{\infty}\frac{d\omega'}{\pi}\frac{\mathrm{Re}[\sigma(\omega')]}{\omega' - \omega}, \tag{35}$$

where $P$ denotes the principal value of the integration. From this formula, we can see that the real part of the conductivity contains a delta function, $\mathrm{Re}[\sigma(\omega)] = \pi\delta(\omega)$, only when the imaginary part has a pole, $\mathrm{Im}[\sigma(\omega)] = 1/\omega$. Actually, there is a peak at zero

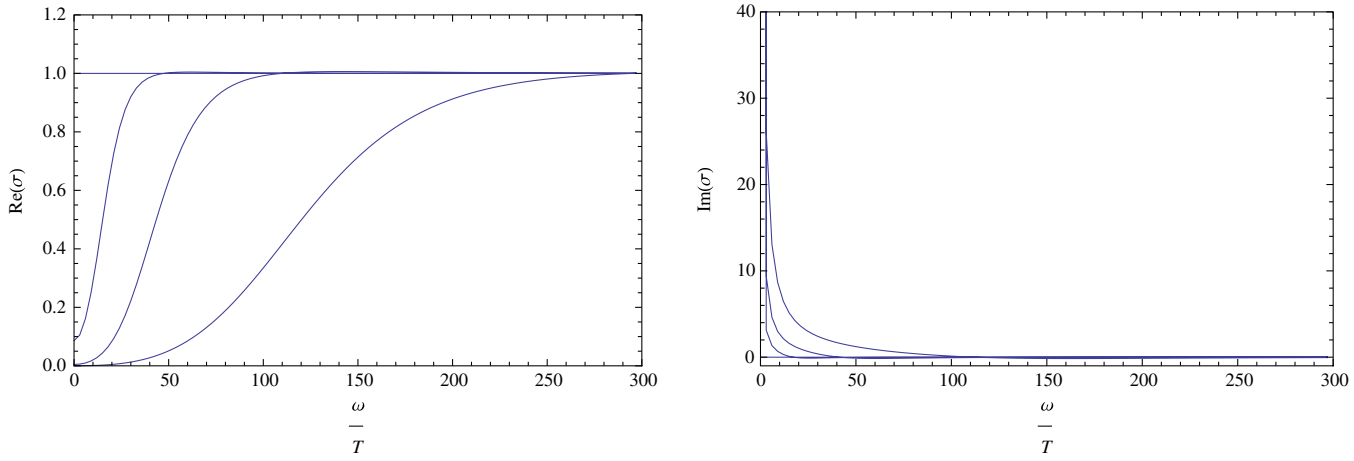


FIG. 5 (color online). The real (imaginary) part of the ac conductivity of the $s$-wave superconductor for the dimension 4 theory at $T/T_c = 1.0, 0.565265, 0.298191, 0.0879648$ from top to bottom (bottom to top).

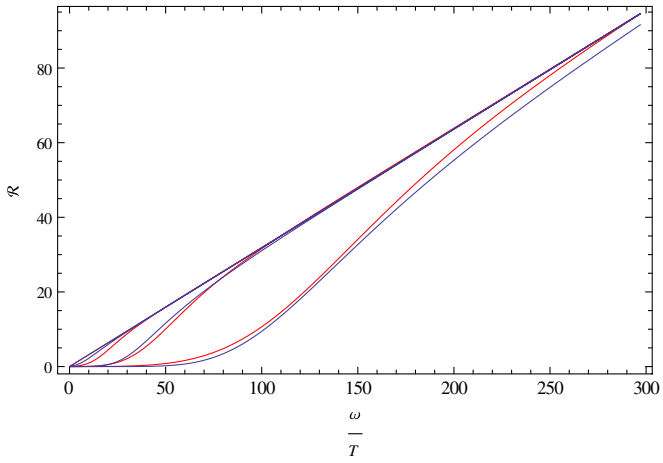


FIG. 6 (color online). The spectral functions of the $s$-wave superconductor for the dimension 3 theory (blue lines) at $T/T_c = 1.0, 0.798694, 0.269798, 0.0864351$ and the dimension 4 theory (red lines) at $T/T_c = 1.0, 0.565265, 0.298191, 0.0879648$ from top to bottom.

frequency for the imaginary part of the conductivity as can be seen in the right plots of Figs. 4 and 5.[4]

In Fig. 6 we plot the results for the spectral function corresponding to the gauge field fluctuation $a_x$. The two figures are consistent with the real part of the conductivity: a gap will appear when the condensate is nonzero (equivalently, when the temperature is low enough) and the spectral functions have a linear behavior with respect to the frequency at large $\omega/T$ (which corresponds to large $\omega/T$ behavior of the conductivity).

## IV. HOLOGRAPHIC *P*-WAVE SUPERCONDUCTORS WITH LIFSHITZ SCALING

In this section we present the results of the $p$-wave superconductor in the Lifshitz black hole background. The structure of this section is the same as the previous one.

### A. Solution for the background fields

As we have seen in the last section, the $s$-wave holographic superconductor is very simple and also elegant in describing some important features of superconductors. However, the Abelian-Higgs model for the $s$-wave superconductor appears to be less universal: we have to specify a potential for the scalar. On the other hand, the $p$-wave superconductor has already been observed in some experiments of condensed matter physics. It is natural as well as interesting to extend the construction of holographic $s$-wave superconductors to the $p$-wave situation. This has been achieved in Ref. [4] by introducing the SU(2) gauge field into the $AdS_4$ black hole background.[5] In this $p$-wave model the chemical potential and the order parameter have been unified into one field, the non-Abelian gauge field, and the action is uniquely determined by gauge invariance. In this sense, the $p$-wave holographic superconductor is more universal than the Maxwell-Scalar system for the $s$-wave superconductor. The action is simply of the form

$$S = \frac{1}{2\kappa^2}\int d^4x\sqrt{-g}\left[R + \frac{6}{L^2} - \frac{1}{4}F^a_{\mu\nu}F^{a\mu\nu}\right], \qquad (36)$$

[4]In fact, we can explicitly plot the delta peak in the real part of the conductivity. However, when carrying out the numerical calculations, it is a little hard because we find that this peak will appear at about $\omega \sim 10^{-20}$ and the numerical computations are not stable there.

[5]Another approach to $p$-wave superconductor where the boundary field theory is known is based on D-brane probe in black brane geometry [19].

where the $SU(2)$ gauge field strength is defined as $F^a_{\mu\nu} = \partial_\mu A^a_\nu - \partial_\nu A^a_\mu + \epsilon^{abc} A^b_\mu A^c_\nu$. The Yang-Mills equation for the gauge field is

$$\partial_\mu(\sqrt{-g}F^{a\mu\nu}) + \sqrt{-g}\epsilon^{abc}A^b_\mu F^{c\mu\nu} = 0. \quad (37)$$

The gauge field ansatz is taken as

$$A = \phi(u)\tau^3 dt + \psi(u)\tau^1 dx, \quad (38)$$

where $\tau^a$ is the generator of the $SU(2)$ gauge group. Plugging this ansatz into the Yang-Mills equation (37) results in

$$\phi'' + \frac{z-1}{u}\phi' - \frac{\psi^2}{f(u)}\phi = 0, \quad (39)$$

and

$$\psi'' + \left[\frac{f'(u)}{f(u)} + \frac{1-z}{u}\right]\psi' + \frac{u^{2z-2}\phi^2}{f(u)^2}\psi = 0. \quad (40)$$

As in the $s$-wave model, boundary behavior of the background fields $\phi(u)$ and $\psi(u)$ is listed as below having chosen $z = 2$,

$$\phi(u \to 0) \sim \rho + \mu \log u, \quad (41)$$

$$\psi(u \to 0) \sim \psi^{(0)} + \psi^{(2)}u^2. \quad (42)$$

The logarithmic term appears again for the $\phi$ field, which suggests that we should identify the constant term $\rho$ as the charge density. We also impose $\psi^{(0)}$ to be zero in our numerical calculations to insure that the superconducting phase transition is a spontaneous breaking of the symmetry. Then the value of $\psi^{(2)}$ is proportional to the expectation value of the $p$-wave order parameter, i.e., $\langle \mathcal{O}_2 \rangle \sim \psi^{(2)}$. Our numerical results are plotted in the following figures.

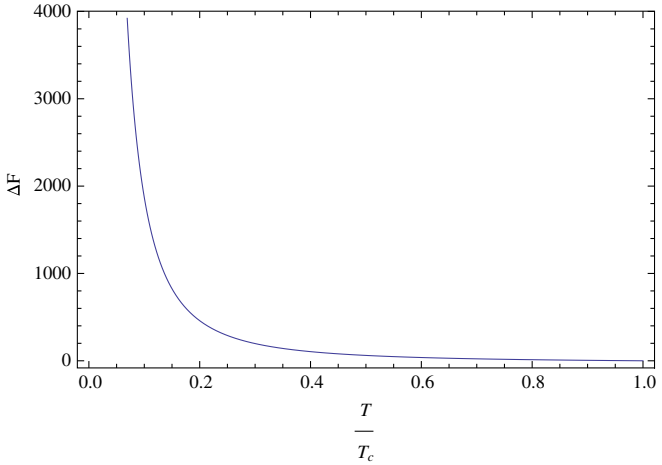


FIG. 7 (color online). The free energy difference between the normal and the superconducting phases for the $p$-wave.

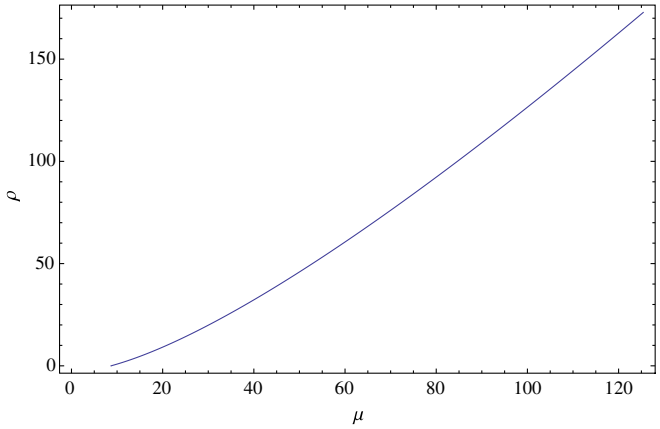


FIG. 8 (color online). Density as a function of $\mu$ for the $p$-wave superconductor.

The free energy difference between the normal and superconducting phases is plotted in Fig. 7. As in the $s$-wave model, the superconducting phase is stable compared to the normal phase when $T < T_c$. The charge density as a function of the chemical potential can be found in Fig. 8. Explicitly, these plots are very similar to the $s$-wave case.

The condensate of the $p$-wave order parameter $\langle \mathcal{O}_2 \rangle$ is plotted in Fig. 9. It is clear to see from this plot that the condensate does not approach some fixed value when $T \to 0$, which is the same as the results of the $s$-wave model mentioned in the last section. Once again, this value is much larger than that of the AdS superconductor. By fitting the curve near the phase transition, we find a mean-field behavior for the condensate,

$$\langle \mathcal{O}_2 \rangle \approx (17.8217T_c)^2(1 - T/T_c)^{1/2} \quad \text{when } T \to T_c, \quad (43)$$

where the critical temperature is $T_c \approx 0.0367064\mu$.

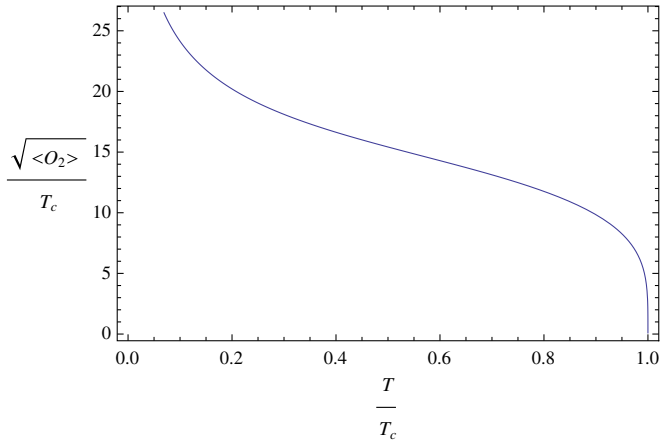


FIG. 9 (color online). The condensate $\langle \mathcal{O}_2 \rangle$ of the $p$-wave superconductor.

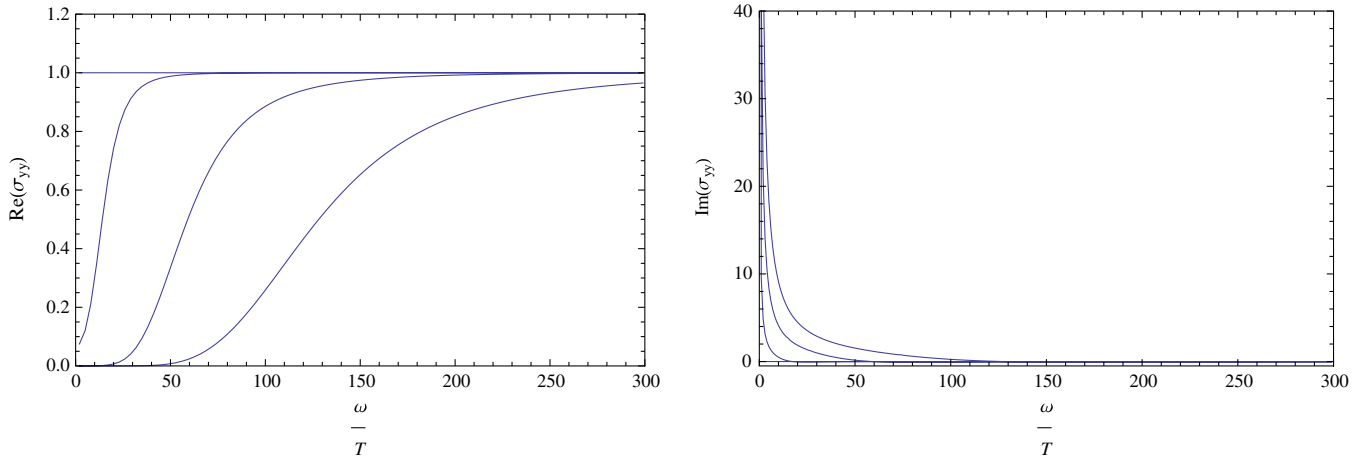


FIG. 10 (color online). The real (imaginary) part of the ac conductivity along the $y$ direction of the $p$-wave superconductor at different temperature $T/T_c = 1.0, 0.588587, 0.171829, 0.079889$ from top to bottom (bottom to top).

### B. Fluctuation analysis: ac conductivities and spectral functions

Owing to the appearance of the background for the gauge field, say $A_0^3$, the SU(2) gauge symmetry is explicitly broken to the $U(1)_3$ generated by the rotation in the colored 12 plane. This residual symmetry is identified as the electromagnetic symmetry. For the conductivity, we need to perturb the system and investigate its linear response. The conductivity of the $p$-wave superconductor is anisotropic, which makes the fluctuation analysis more complicated than the $s$-wave case. We here focus on the decoupled mode $a_y^3(t, u)$, decoupled sector $\{a_x^1(t, u), a_t^2(t, u), a_x^3(t, u)\}$ and leave the full fluctuation analysis including spatial momentum for future investigations.

For the fluctuation mode $a_y^3(t, u) \sim e^{-i\omega t} a_y^3(u)$, which is decoupled from other modes, we have the following equation:

$$a_y^{3\prime\prime} + \left[\frac{f(u)'}{f(u)} - \frac{z-1}{u}\right] a_y^{3\prime} + \left[\frac{u^{2z-2}\tilde{\omega}^2}{f(u)^2} - \frac{\psi^2}{f(u)}\right] a_y^3 = 0. \tag{44}$$

This mode looks like the electromagnetic fluctuation in the scalar system for the $s$-wave model and the procedure for numerical computation of the conductivity along the $y$ direction is of course in parallel with the $s$-wave situation. We here only present the final results for the conductivity in Fig. 10.

We then move on to the conductivity along the $x$ direction. For this purpose, one should analyze the fluctuations $\{a_t^1(t, u), a_t^2(t, u), a_x^3(t, u)\} \sim e^{-i\omega t}\{a_t^1(u), a_t^2(u), a_x^3(u)\}$, which is also decoupled from other modes but is self-coupled. There are three coupled equations of second order,

$$\begin{aligned}
&a_t^{1\prime\prime} + \frac{z-1}{u} a_t^{1\prime} + \frac{\phi\psi}{f(u)} a_x^3 = 0,\\
&a_t^{2\prime\prime} + \frac{z-1}{u} a_t^{2\prime} - \frac{\psi}{f(u)}(i\tilde{\omega} a_x^3 + \psi a_t^2) = 0,\\
&a_x^{3\prime\prime} + \left[\frac{f(u)'}{f(u)} + \frac{1-z}{u}\right] a_x^{3\prime}\\
&\quad - \frac{u^{2z-2}}{f(u)^2}(-\tilde{\omega}^2 a_x^3 + \phi\psi a_t^1 + i\tilde{\omega}\psi a_t^2) = 0,
\end{aligned} \tag{45}$$

and two constraints of first order,[6]

$$\begin{aligned}
&i\tilde{\omega} a_t^{1\prime} + \phi a_t^{2\prime} - \phi' a_t^2 = 0,\\
&-i\tilde{\omega} a_t^{2\prime} + \phi a_t^{1\prime} - \phi' a_t^1 + \frac{f(u)}{u^{2z-2}}(\psi a_x^{3\prime} - a_x^3\phi') = 0.
\end{aligned} \tag{46}$$

Near the horizon $u = 1$, we choose the ingoing wave boundary condition for different modes and also impose that the time components vanish at the horizon,

$$\begin{aligned}
a_x^3 &= (1-u)^{-i\tilde{\omega}/4}[1 + a_x^{3(1)}(1-u) + a_x^{3(2)}(1-u)^2\\
&\quad + a_x^{3(3)}(1-u)^3 + \cdots],\\
a_t^1 &= (1-u)^{-i\tilde{\omega}/4}[a_t^{1(1)}(1-u) + a_t^{1(2)}(1-u)^2\\
&\quad + a_t^{1(3)}(1-u)^3 + \cdots],\\
a_t^2 &= (1-u)^{-i\tilde{\omega}/4}[a_t^{2(1)}(1-u) + a_t^{2(2)}(1-u)^2\\
&\quad + a_t^{2(3)}(1-u)^3 + \cdots],
\end{aligned} \tag{47}$$

where we have used the linearity of Eqs. (45) to set the scale of $a_x^3$ at the horizon to 1. The coefficients in the above expansions can be fully determined by plugging the

[6]These constraints come form the radial gauge we have chosen for the gauge field fluctuation, i.e., $a_u^a = 0$ when deriving the equations of motion.

expansion into Eqs. (45) and counting powers of $(1-u)$. Then, Eq. (47) can provide initial conditions for these second order differential equations (45). In fact, we use these power solutions to do numerical integration from the horizon to the conformal boundary as mentioned in the last section.

At the conformal boundary, the general solutions to Eq. (45) are of the form

$$\begin{aligned} a_t^1 &= A_t^{1(0)} + A_t^{1(1)} \log u + \cdots, \\ a_t^2 &= A_t^{2(0)} + A_t^{2(1)} \log u + \cdots, \\ a_x^3 &= A_x^{3(0)} + A_x^{3(1)} u^2 + \cdots. \end{aligned} \tag{48}$$

We can also expand the constraint equations near the conformal boundary, but it is of no use for later calculations.

As argued in Ref. [4], for the conductivity to be a gauge invariant quantity, we need to construct a new mode from $a_t^1$, $a_t^2$, $a_x^3$ which should be invariant under the gauge transformation that respects our gauge choice. We here do not go into the details of the construction of this field but write down the mode directly,

$$\tilde{a}_x^3 \equiv a_x^3 + \psi \frac{i\tilde{\omega} a_t^2 + \phi a_t^1}{\phi^2 - \tilde{\omega}^2}. \tag{49}$$

Plugging the boundary behavior as in Eq. (48) into the newly defined mode and expanding it near the conformal boundary,

$$\tilde{a}_x^3 = \tilde{A}_x^{3(0)} + \tilde{A}_x^{3(1)} u^2 + \cdots, \tag{50}$$

with

$$\tilde{A}_x^{3(0)} = A_x^{3(0)}, \qquad \tilde{A}_x^{3(1)} = \frac{A_t^{1(0)}}{\mu} \psi^{(2)} + A_x^{3(1)}. \tag{51}$$

Then, the conductivity along the $x$ direction is straightforwardly defined as

$$\sigma_{xx}(\omega) = \frac{1}{i\omega} \frac{\tilde{A}_x^{3(1)}}{\tilde{A}_x^{3(0)}}. \tag{52}$$

Notice that the above formula is very different from Eq. (4.19) of Ref. [4] due to the appearance of the logarithmic terms in the time component of the SU(2) gauge field (for both the background and the fluctuations). The definition for the spectral function is similar to the $s$-wave case and we list them in what follows for completeness:

$$\mathcal{R} = -2 \frac{\tilde{A}_x^{3(1)}}{\tilde{A}_x^{3(0)}} \tag{53}$$

along the $x$ direction and

$$\mathcal{R} = -2 \frac{A_y^{3(1)}}{A_y^{3(0)}} \tag{54}$$

along the $y$ direction.

In Fig. 11 we plot numerical results for the conductivity along the $x$ direction. We can see that the results are very similar to those of the $y$ direction stated in Fig. 10. Explicitly, there is a DC infinity in the conductivity along the $x$ direction. What is strikingly different from the $AdS_4$ $p$-wave superconductor is that there is no pole for the imaginary part of the conductivity at nonzero frequency. Mathematically, this is due to the logarithmic term appearing in the boundary behavior for the time component fluctuations of the gauge field. We will take this as the effect of the nontrivial dynamical exponent $z \neq 1$. The real (imaginary) part of the conductivity approaches 1 (0) more slowly than the $y$ direction case, which is consistent with the spectral function profiles plotted in Fig. 12. This can be explained by the anisotropic characteristic of the $p$-wave superconductor.

The qualitative behavior is similar to the corresponding $s$-wave case: at high frequency the real part of the conductivity approaches 1 while the imaginary part goes to 0;

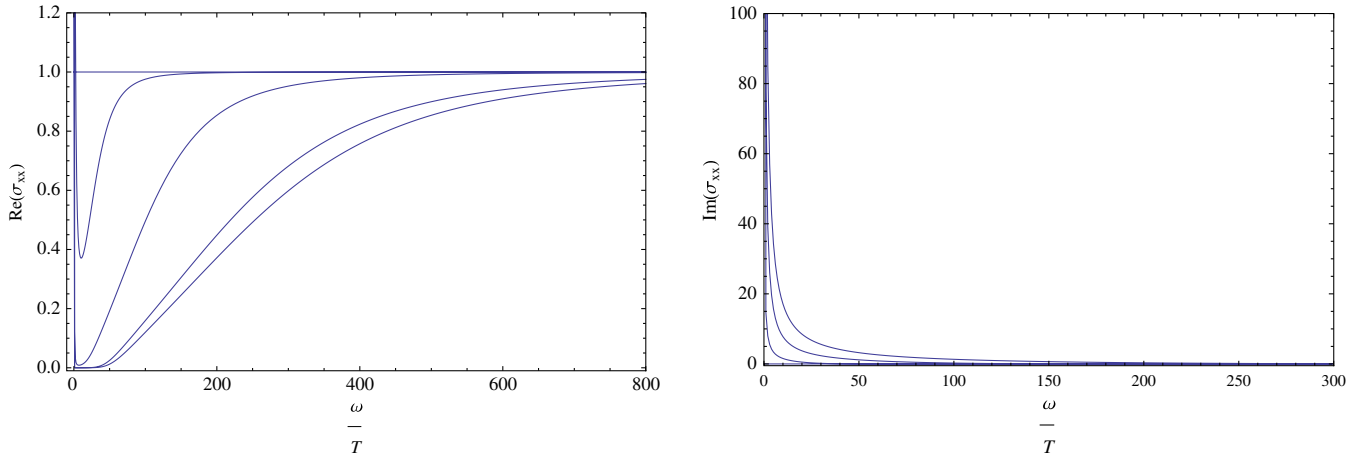


FIG. 11 (color online). The real (imaginary) part of the ac conductivity along $x$ direction of the $p$-wave superconductor at $T/T_c = 1.0, 0.588587, 0.171829, 0.079889, 0.0691493$ from top to bottom (bottom to top).

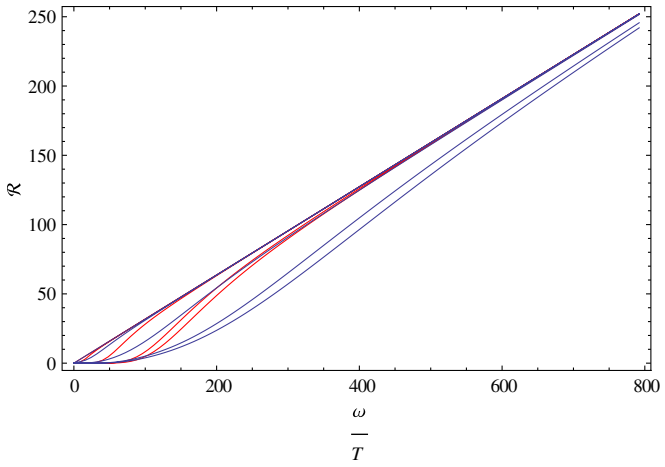


FIG. 12 (color online). The spectral functions for the modes $a_y^3$ (red lines) and $\tilde{a}_x^3$ (blue lines) at temperature corresponding to the conductivity pictures.

a peak also appears at zero frequency, indicating a DC superconductivity; and the gap forms as the temperature decreases and it gets increasingly deep until the conductivity is exponentially small. The appearance of the delta peak at zero frequency can also be well understood by the Kramers-Krönig relation (35). Although the conductivity $\sigma_{yy}(\omega)$ behaves qualitatively similar to $\sigma_{xx}(\omega)$, the anisotropic characteristic of the $p$-wave superconductor can also be seen from the two conductivities: the real part of the $\sigma_{xx}(\omega)$ grows much slowly than that of $\sigma_{yy}(\omega)$. These features are common with the AdS superconductors. One main difference is that there is no pole at nonzero frequency for the imaginary part of $\sigma_{xx}(\omega)$ as mentioned before. Another main difference from the AdS black hole superconductor is that the imaginary part of the conductivity never goes below zero and approaches zero quite slowly.

## V. SUMMARY

In this work we explored properties of holographic superconductors with nontrivial dynamical exponents by putting the Abelian-Higgs model ($s$-wave) or SU(2) gauge field ($p$-wave) into the Lifshitz black hole geometry constructed in Ref. [6]. We found that the order parameters $\langle \mathcal{O} \rangle$ all have mean-field behavior $(T - T_c)^{1/2}$ near the critical temperature $T_c$, which is qualitatively consistent with the AdS superconductors as well as BCS theory. One difference between our results and previous investigations on condensates is that the condensates do not approach some fixed values in the zero temperature limit.[7] We then plot the free energy difference between the normal and superconducting phases, which can be taken as evidence of the occurrence of the superconducting phase transition. We also numerically compute the ac conductivities and they nearly behave in the same way: a peak appears at zero frequency, indicating a DC superconductivity; and the gap forms as the temperature decreases and it gets increasingly deep until the real part of the conductivity gets exponentially small. The anisotropic characteristic of the $p$-wave superconductor can be seen from the difference between $\sigma_{xx}(\omega)$ and $\sigma_{yy}(\omega)$: when increasing the frequency $\omega$, the rates of the real parts of ac conductivities, $\sigma_{xx}$ and $\sigma_{yy}$, increase. But we do not see a pole at nonzero frequency for the imaginary part of $\sigma_{xx}(\omega)$, which does exist in the $p$-wave superconductor when using the $AdS_4$ black hole geometry. Another feature is that all the real parts of the conductivities approach 1 (but never exceed this value) in contrast to those of the AdS case. With respect to this, the imaginary parts of the conductivities approach zero in the high frequency limit but never go below zero. We attribute these differences from the AdS case to the effect of the nontrivial dynamical exponent. More specifically, the black hole geometry considered in this work is anisotropic between space and time, very different from the Schwarzschild-AdS black hole, which results in different asymptotic behaviors of temporal and spatial components of gauge fields than previously concluded in the Schwarzschild-AdS black hole. These common features also imply that general gauge/gravity duality is a useful and powerful tool in producing some universal properties of strongly coupled system in condensed matter physics.

## ACKNOWLEDGMENTS

The author would like to thank Johanna Erdmenger, Jonathan Shock, Xin Gao and Da-Wei Pang, and Xu Zhang for useful discussions. This work was supported by the MPS-CAS Doctoral Training Program.

[7]We would like to state that this feature is not due to the numerical approach used here. Actually, we already used our numerical method to carry out similar computations in other black hole backgrounds of the asymptotic AdS type and found that the condensed operator approached a constant value. Therefore, we conclude that the feature found here is due to the nontrivial dynamical exponent $z$.

[1] J. M. Maldacena, Adv. Theor. Math. Phys. **2**, 231 (1998).
[2] J. Erdmenger, N. Evans, I. Kirsch, and E. Threlfall, Eur. Phys. J. A **35**, 81 (2008); S. S. Gubser and A. Karch, Annu. Rev. Nucl. Part. Sci. **59**, 145 (2009); S. A. Hartnoll, Classical Quantum Gravity **26**, 224002 (2009); C. P. Herzog, J. Phys. A **42**, 343001 (2009); U. Gursoy, Mod. Phys. Lett. A **23**, 3349 (2008); J. McGreevy, Adv. High Energy Phys. **2010**, 1 (2010).

[3] S. A. Hartnoll, C. P. Herzog, and G. T. Horowitz, Phys. Rev. Lett. **101**, 031601 (2008); J. High Energy Phys. 12 (2008) 015.

[4] S. S. Gubser and S. S. Pufu, J. High Energy Phys. 11 (2008) 033.

[5] S. Kachru, X. Liu, and M. Mulligan, Phys. Rev. D **78**, 106005 (2008).

[6] G. Bertoldi, B. A. Burrington, and A. Peet, Phys. Rev. D **80**, 126003 (2009); M. Taylor, arXiv:0812.0530.

[7] P. Kovtun and D. Nickel, Phys. Rev. Lett. **102**, 011602 (2009); D.-W. Pang, J. High Energy Phys. 01 (2010) 120; E. Brynjolfsson, U. Danielsson, L. Thorlacius, and T. Zingg, J. High Energy Phys. 08 (2010) 027; T. Nishioka and H. Tanaka, J. High Energy Phys. 02 (2011) 023; S. A. Hartnoll, D. M. Hofman, and D. Vegh, J. High Energy Phys. 08 (2011) 096; J. P. Lemos and D.-W. Pang, J. High Energy Phys. 06 (2011) 122; L. Huijse, S. Sachdev, and B. Swingle, Phys. Rev. B **85**, 035121 (2012); Y. S. Myung, arXiv:1203.1367v2.

[8] S. A. Hartnoll, J. Polchinski, E. Silverstein, and D. Tong, J. High Energy Phys. 04 (2010) 120.

[9] T. Azeyanagi, W. Li, and T. Takayanagi, J. High Energy Phys. 06 (2009) 084.

[10] L. Q. Fang, X.-H. Ge, and X.-M. Kuang, arXiv:1201.3832; M. Alishahiha, M. M. Mozaffar, and A. Mollabashi, arXiv:1201.1764.

[11] S.-J. Sin, S.-S. Xu, and Y. Zhou, Int. J. Mod. Phys. A **26**, 4617 (2011).

[12] E. Brynjolfsson, U. H Danielsson, L. Thorlacius, and T. Zingg, J. Phys. A **43** 065401 (2010).

[13] R.-G. Cai and H.-Q. Zhang, Phys. Rev. D **81**, 066003 (2010).

[14] U. H. Danielsson and L. Thorlacius, J. High Energy Phys. 03 (2009) 070; R. B. Mann, J. High Energy Phys. 06 (2009) 075; D.-W. Pang, arXiv:0905.2678; D.-W. Pang, J. High Energy Phys. 10 (2009) 031; K. Balasubramanian and J. McGreevy, Phys. Rev. D **80**, 104039 (2009); E. Ayon-Beato, A. Garbarz, G. Giribet, and M. Hassaine, Phys. Rev. D **80**, 104029 (2009); R.-G. Cai, Y. Liu, and Y.-W. Sun, J. High Energy Phys. 10 (**2009**) 080; Y. S. Myung, Y.-W. Kim, and Y.-J. Park, Eur. Phys. J. C **70**, 335 (2010); D.-W. Pang, J. High Energy Phys. 01 (2010) 116; K. Goldstein, S. Kachru, S. Prakash, and S. P. Trivedi, J. High Energy Phys. 08 (2010) 078; E. Ayon-Beato, A. Garbarz, G. Giribet, and M. Hassaine, J. High Energy Phys. 04 (2010) 030; J. Blaback, U. H. Danielsson, and T. Van Riet, J. High Energy Phys. 02 (2010) 095; Y. S. Myung, Phys. Lett. B **690**, 534 (2010).

[15] C.-M. Chen and D.-W. Pang, J. High Energy Phys. 06 (2010) 093; K. Balasubramanian and K. Narayan, J. High Energy Phys. 08 (2010) 014; K. Goldstein, N. Iizuka, S. Kachru, S. Prakash, S. P. Trivedi, and A. Westphal, J. High Energy Phys. 10 (2010) 027; R. Gregory, S. L. Parameswaran, G. Tasinato, and I. Zavala, J. High Energy Phys. 12 (2010) 047; M. Dehghani, R. Mann, and R. Pourhasan, Phys. Rev. D **84**, 046002 (2011); D. Cassani and A. F. Faedo, J. High Energy Phys. 05 (2011) 013; I. Amadoand and A. F. Faedo, J. High Energy Phys. 07 (2011) 004; J. Tarrio and S. Vandoren, J. High Energy Phys. 09 (2011) 017; S. F. Ross, Classical Quantum Gravity **28**, 215019 (2011); X. Dong, S. Harrison, S. Kachru, G. Torroba, and H. Wang, J. High Energy Phys. 06 (2012) 041; Y. Liu, J. High Energy Phys. 06 (2012) 024; L. Barclay, R. Gregory, S. Parameswaran, G. Tasinato, and I. Zavala, J. High Energy Phys. 05 (2012) 122.

[16] S. S. Gubser, Phys. Rev. D **78**, 065034 (2008).

[17] I. R. Klebanov and E. Witten, Nucl. Phys. **B556**, 89 (1999).

[18] D. T. Son and A. O. Starinets, J. High Energy Phys. 09 (2002) 042.

[19] M. Ammon, J. Erdmenger, M. Kaminski, and P. Kerner, Phys. Lett. B **680**, 516 (2009); M. Ammon, J. Erdmenger, M. Kaminski, and P. Kerner, J. High Energy Phys. 10 (2009) 067; P. Basu, J. He, A. Mukherjee, and H.-H. Shieh, J. High Energy Phys. 11 (2009) 070; K. Peeters, J. Powell, and M. Zamaklar, J. High Energy Phys. 09 (2009) 101.